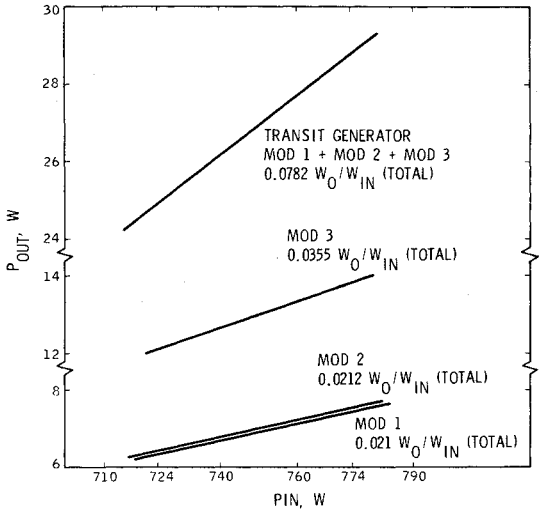

Fig. 7 Power output vs power input (QM-III generator).

and 116), and the data received from the generator flying on Transit (point 260 observed at 01.58). The comparison was made at an output current value of 6.30 amp and at a hot junction temperature of 400°C. In both cases, the power output was normalized for a ΔT of 265°C. In the case of the flight-type panels, the values were extrapolated to a hypothetical generator assembled with 12 panels. At JPL, Group M1 was operated under the following conditions: $\bar{T}_h = 400$°C, $\bar{T}_c = 147.2$°C, $\bar{\Delta T} = 253.3$°C, output voltage 1.180 v, output current 6.30 amp. For a 12-panel generator (hypothetical), the power output normalized for a $\bar{\Delta T} = 265$°C was 33 w with an output voltage $\Sigma_{12} = 4.72$ v. The generator on the Transit satellite had the following characteristics: $\bar{T}_h = 399.7$°C, $\bar{T}_c = 133.3$°C, $\Delta T = 266.4$°C, and $V_o = 5.581$ v. The output power normalized to $\Delta T = 265$°C was 35.6 w or 2.6 w higher than that extrapolated from the data observed at JPL from Group 1.

Life Test

After the 502 hr of operation required to perform the parametric test, the generator was adjusted for operation in a long-term life test mode. The conditions for this operation at BOL are $P_{in} = 744$ w, $\bar{T}_h = 400$°C nom. (for flight-type panels), $\bar{T}_c = 151.8$°C, $\bar{\Delta T} = 250.6$°C, $I_L = 5.301$ amp, $E_L = 1.40$ v, $P_o = 7.423$ v, normalized output power $P_{o265} = 33.20$ w. At the same input power and output voltage, Group 2 (new cold-pressed panels) operated at a $\bar{T}_h = 400.8$, $\bar{T}_c = 154.0$, $\bar{\Delta T} = 246.8$, $I_L = 5.354$ amps, while Group 3 (composed of used panels) for the same input power operated at $\bar{T}_h = 404.5$, $\bar{T}_c = 158.1$ $\Delta T = 246.3$, $V_L = 2.60$ v, and $I_L = 5.324$ amp.

The life test is performed at a fixed and constant output voltage from each group of panels and the input power is periodically decreased to follow the radioisotope decay scheme. At present, the generator has operated at JPL for a total accrued time of 4000 hr. During this time the degradation in output power of the different modules and that of the generator as a whole was calculated as: $M_1 = 1.25\%/1000$ hr, $M_2 = 2.21\%/1000$ hr, $M_3 = 1.44\%/1000$ hr, and generator total $= 1.6\%/1000$ hr. These values include both the material bulk property changes and the effects of the reduction in input power, simulating the isotope decay scheme. Discounting the latter indicates that the changes in thermoelectric material bulk properties *only* are $M_1 = 1\%/1000$ hr, $M_2 = 2.04\%/1000$ hr, $M_3 = 1.224\%/1000$ hr, generator total $= 1.37\%/1000$ hr. It should be remembered that M_1 was assembled with materials made by the warm vacuum-pressed process while M_2 and M_3 used couples made by the cold-press process. The difference between M_2 and M_3 is that M_2 was assembled with new material which had not experienced the "burn in" settling period, while the materials used in M_3, having been tested previously for long time periods, were settled and are more representative of the behavior of the cold pressed material.

Conclusions

A thermoelectric generator similar to the generator flown on Transit and assembled with 12 Isotec-type panels, three of which represent flight hardware, is presently on test at JPL. After extensive parametric tests, the generator is operating in a long-term life test mode, during which the input power will be reduced to simulate the radioisotopic decay. The panels in the test generator are electrically grouped as three independent generators, each with its independent load circuit. The life test is conducted at a constant output voltage from each group of panels. Comparison made between the data received from the generator mounted on the Transit spacecraft and the results observed at JPL from the group composed of the flight-type panels (extrapolated to 12 panels) indicated that for a normalized $\Delta T = 265$°C, the output of the test panels is slightly lower than that recorded from the flight generator.

References

[1] Bradshaw, G. and Postula, F., "Description and Status of the Transit Thermoelectric Converter," *7th IECEC Proceedings*, Sept. 1972, pp. 200–215.

Aerodynamic Heat Transfer to RSI Tile Surfaces and Gap Intersections

JAMES C. DUNAVANT* AND DAVID A. THROCKMORTON†
NASA Langley Research Center, Hampton, Va.

THE design of a space shuttle orbiter, reusable for a hundred or more missions, dictates that the thermal protection system be lightweight, reliable, and last for many missions with minimal costs for refurbishment.[1] As currently envisioned, most of the orbiter surface will be covered with a nonmetallic, low-density refractory oxide. This material, referred to by the acronym RSI (Reusable Surface Insulation), both withstands (without degradation) the high heating rates and temperatures of repeated missions, and insulates the cold structure of the shuttle from the re-entry environment.[2] The material will be attached to the surface in 6-in. square tiles which vary in thickness from about $\frac{1}{2}$-in. in the low heating areas to 3 in. where the heating is intense. Small gaps between the tiles will allow for differential expansions which result from the many varied thermal conditions to which the exterior surface and bondline between the tile and structural interface are exposed during a mission.[3] Heating inside the gaps and the change in the surface aerodynamic heating characteristics which results from the presence of the gaps are of serious concern to the designer and are the subject of this Note.

Aerothermal heating tests of a simulated RSI tile array were made on the sidewall of the Langley Research Center's Mach 10 Continuous Flow Hypersonic Tunnel[4] where the wall boundary layer was used to simulate a thick turbulent boundary-layer condition on the orbiter. The tile array, shown schematically in Fig. 1, consisted of actual RSI tiles 2.55 in. thick,

Received December 6, 1973.
Index categories: Boundary Layers and Convective Heat Transfer—Turbulent; LV/M Aerodynamic Heating; Entry Vehicles and Landers.

* Head, Thermal Analysis Section, Space Systems Division. Member AIAA.
† Aero-Space Technologist, Thermal Analysis Section, Space Systems Division.

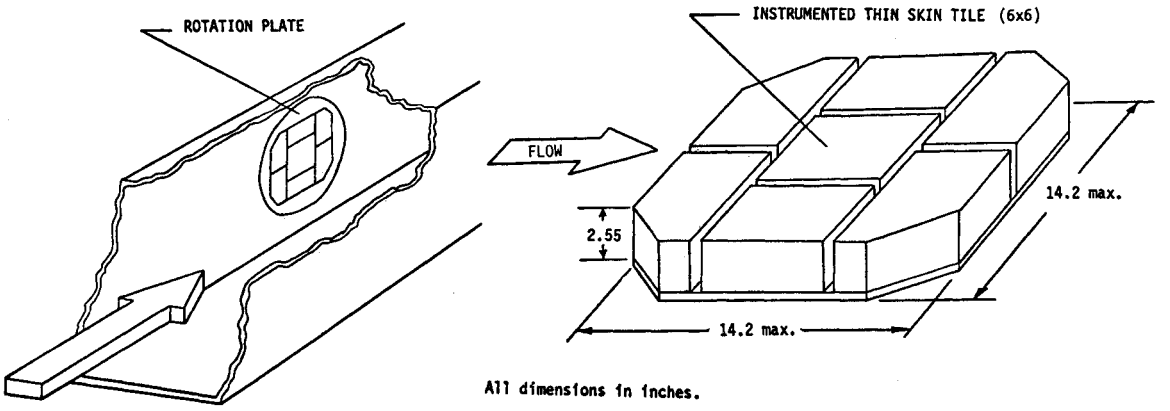

Fig. 1 Simulated tile array model schematic.

surrounding a metal thin-skin tile which contained thermocouples for measurement of heating rates. Gap widths from 0.05-in. to 0.28-in. were set for the tests, and heating at several flow orientations was obtained by rotating the tile array in the sidewall mount. The effects of tile thickness mismatch were observed by setting the instrumented tile 0.100 in. above and 0.066 in. below the surrounding tiles. The tests were conducted at a freestream Reynolds number of 10^6 per ft.

Contours of heat-transfer coefficient, h, are shown for flush and protruding tile conditions in Fig. 2. The data are normalized to an undisturbed heating rate, h_{surf}, measured on a flat plate (without gaps) at a reference point on the sidewall centerline corresponding to the forward edge of the tile. For the flush-mounted tile, the heating decayed rapidly with distance into the gap as shown in Fig. 2a, for the largest tested gap (0.28 in.). On the tile surface, heating rates as high as 75% above the reference, undisturbed value were measured. No appreciable increase in heating is shown where the boundary-layer bridges the gap and reattaches at the forward lip of the tile. The average heating rate to the surface was 24% greater than that to the same area on the undisturbed plate. For other flow orientations, the reattachment heating rates were a maximum of twice the reference value; the increase in heating at the center of the nonalined tiles was between 15% and 24%. As expected, surface mismatch causes the worst heating condition with heating rates as high as three times the undisturbed value measured on the 0.1-in. protruding tile, Fig. 2b; average heating to the tile was increased an additional 30% over the flush tile.

A number of tile arrangements are possible; tiles can be arranged so that the gaps form a orthogonal grid or, as currently most prominently considered, in a "brickyard" array, Fig. 1. This array avoids the longitudinal gap alinement of the orthogonal grid and limits the streamwise gap to one tile length or 6 in. At the end of each streamwise gap, the flow inside the longitudinal gap either turns 90° into the spanwise gaps or spills out over the tile outer surface. On the upstream tile face at the gap intersection, a region of intense heating was expected. The present tests failed to show this expected heating increase whereas results from tests by Johnson[5] and Lockman of the Ames Research Center (unpublished) have shown heating up to 14

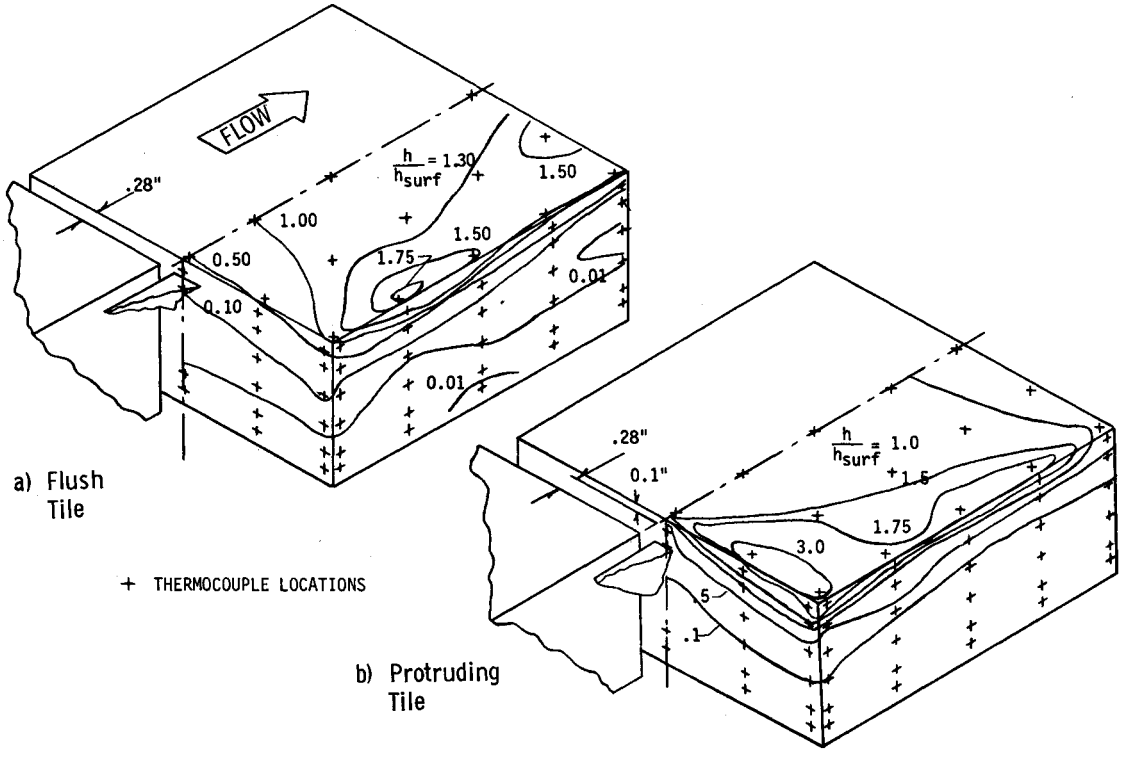

Fig. 2 Heat transfer rate contours on RSI tiles. $M = 10$, $R_{\delta^*} \approx 0.4 \times 10^6$.

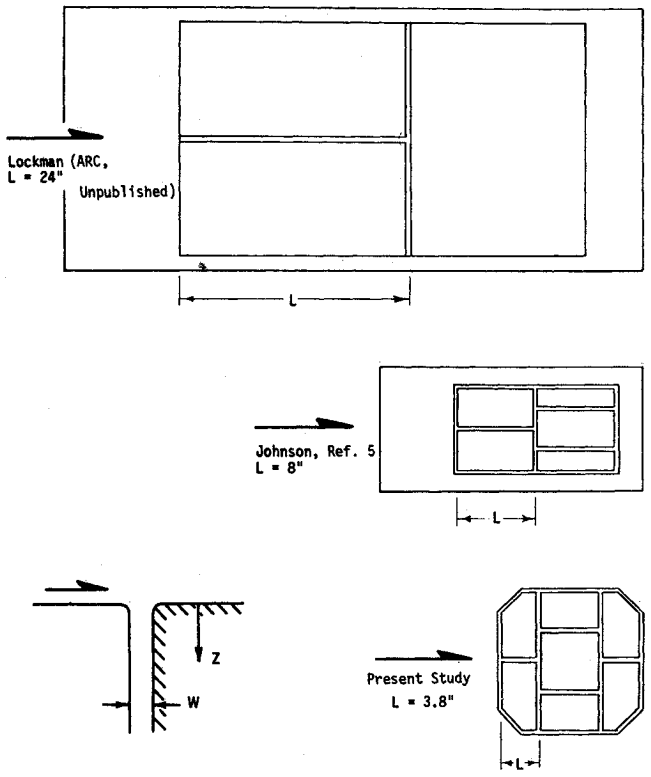

Fig. 3 RSI gap heating test geometries.

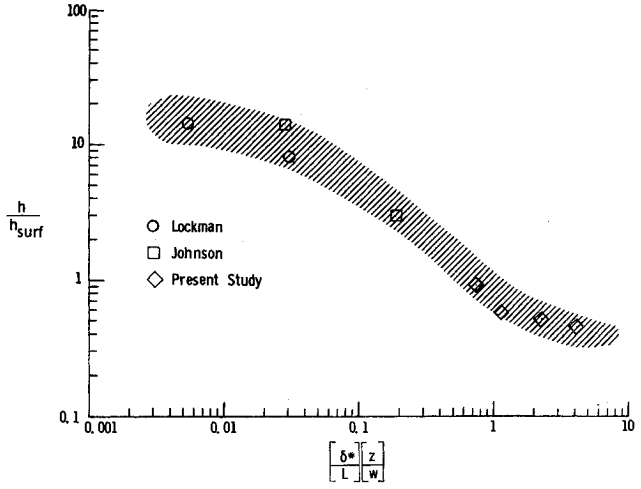

Fig. 4 Heating to transverse gap at streamwise gap intersection.

times the undisturbed surface value. The planform geometries of the three investigations are shown to the same scale in Fig. 3; longitudinal gap lengths varied from Lockman's high value of 24 in. to 3.8 in. for the present investigation, none of the models had the correct gap length of 6 in. Boundary-layer displacement thickness, δ^*, varied widely among these tests for a maximum of 4.75 in. for tests run on the tunnel sidewalls to a minimum of 0.15 in. where the model was positioned in the freestream (see Table 1).

It seems logical to assume that as streamwise gap length increases, the flow within the gap approaches a fully developed channel flow, and the rate at which this occurs is dependent upon the shear layer stress or the external boundary-layer thickness. The heating level at the intersection of the streamwise and transverse gaps is expected to be proportional to the development of the streamwise gap flow. This hypothesized effect of gap flow development on the intersection heating is supported by the correlation of the heating increase with boundary-layer thickness, gap length, and depth into the gap shown in Fig. 4. This correlation may be restricted to the range of data which are limited. However, the data do cover some relevent orbiter flight conditions. As an example, the correlation suggests that at a position one gap width below the mold line surface ($Z/W = 1$), the 6-in. long gap will produce no heating increase if the boundary-layer displacement thickness is more than 4 in. (which, in hypersonic flight, may be expected at many locations on a vehicle as large as the shuttle). However, in surface areas where the displacement thickness is as little as 1 in., the

Table 1 Gap intersection heating data for Fig. 4.

MACH NO.	DATA		δ^*	L	$\frac{\delta^*}{L}$	w	z	$\frac{z}{w}$	$\frac{\delta^*}{L}\frac{z}{w}$	$\frac{h}{h_{surf}}$†	MODEL LOCATION
7.4	Lockman (ARC, Unpublished)	○	.25	24	.0104	.100	.052	.52	.0054	14.4	Free Stream
			.25	24	.0104	.100	.296	2.96	.0308	8.21	Free Stream
8	Johnson, Ref. 5	□	1.00	8	.1250	.125	.1875	1.50	.1875	3.09	Tunnel Wall
			.15	8	.0188	.125	.1875	1.50	.0282	14.2	Free Stream
10	Present Study	◇	4.75	3.8	1.250	.050	.163	3.26	4.08	.464	Tunnel Wall
						.090	.163	1.81	2.26	.530	
						.180	.163	.906	1.13	.594	
			4.75	3.8	1.250	.280	.131	.582	.726	.956	Tunnel Wall

†Reference values of h_{surf} used to non-dimensionalize the data are as follows:
Johnson - Average measured value to surface of tile array.
Lockman - Computed value to surface of a flat plate under laminar flow conditions.
Present Study - Measured value to surface of smooth flat plate on tunnel wall.

All dimensions in inches.

intersection gap heating may be three times the surface heating.

In summary, the results of the experimental study show that the heating to RSI tile surfaces is significantly increased in some areas. As would be expected, the largest increase occurs on a tile which protrudes above the others. Heating on the upstream face of a tile is strongly affected by the interacting longitudinal gap flow. In flight, flow developing in 6-in. long longitudinal gaps is expected to produce heating rates several times the corresponding smooth surface heating rates where the boundary layer is thin, but have little or no effect under thick boundary-layer conditions.

References

[1] Anderson, R. W., Brooks, W. A., Jr., Leonard, R. W., and Maltz, J., "Shuttle, Structures—A Technology Overview," *Astronautics and Aeronautics*, Vol. 9, No. 2, Feb. 1971, pp. 38–47.

[2] Hello, S., "The Space Shuttle Program—Progress and Plans," AIAA/ASME/SAE 14th Structures Structural Dynamics and Materials Conference, March 20–22, 1973, Williamsburg, Va.

[3] Love, E. S., "Advanced Technology and the Space Shuttle," *Astronautics and Aeronautics*, Vol. 11, No. 2, Feb. 1973, pp. 30–66.

[4] Dunavant, J. C. and Stone, H. W., "Effects of Roughness on Heat Transfer to Hemisphere Cylinders at Mach Numbers 10.4 and 11.4," TN D-3871, March 1967, NASA.

[5] Johnson, C. B., "Heat Transfer Data to Cavities Between Simulated RSI Tiles at Mach 8," CR-128, 770, June 1973, (Space Shuttle DMS-DR-2043), NASA.

Correlation of Radiative Heating Calculations for Venus Entry

C. T. EDQUIST*

Martin Marietta Corporation, Denver, Colo.

ESTIMATES of the effect of configuration and trajectory changes on entry aeroheating are valuable for a quick assessment of possible alternative configurations and/or launch opportunities. The proper correlating parameters for convective heating are well known.[1] Since radiative heating is a significant fraction of the total for Venus entry, a complete assessment of the heat shield design requires a correlation of the radiative as well as the convective heat load.

Entry heating calculations have been performed for a number of configuration and trajectory combinations in support of a Venus entry study.[2] Table 1 lists the entry velocity V_E, entry angle γ_E, ballistic coefficient β, cone angle θ_c, and nose radius R_n for each of the cases examined. The basic shape considered was a sphere-cone but three Apollo-like configurations, essentially spherical segments, were also included. The radiative heat flux histories to the wall at the stagnation point and at a forebody point located radially at about two-thirds of the base radius were determined. Although the study was not specifically parametric, a wide enough range of the parameters of interest was included so that correlation of the results could be attempted.

Only a brief description of the calculation procedure[2] will be given here. Basically, an uncoupled analysis was made. That is, convective, radiative, and ablative phenomena were considered separately and then correction factors were applied where appropriate. In this situation, calculation of the radiative flux requires a solution for the inviscid flowfield to provide the necessary shock layer thickness and thermodynamic variables.

Received November 30, 1973; revision received January 31, 1974.
Index category: Radiation and Radiative Heat Transfer.

* Staff Engineer. Member AIAA.

Table 1 Venus trajectory and geometry parameters and radiative heating results

Case	V_E km/s	γ_E deg	β kg/m^2	θ_c deg	R_n m	q_{c_m}' MW/m^2	Q_c' MJ/m^2	q_{r_m}' MW/m^2	Q_r' MJ/m^2
1	11.16	40	78.54	60	0.1586	4.51	9.71	5.85	10.2
2		40	78.54	60	0.3683	7.05	15.0	9.00	16.0
3		40	78.54	60	0.5525	8.58	17.6	10.5	19.5
4		40	78.54	55	0.5080	8.35	17.7	7.80	14.6
5		40	78.54	70	0.3683	8.00	16.9	13.2	26.0
6		40	78.54	AP	1.585	15.7	31.0	13.7	25.1
7		40	78.54	AP	2.378	18.6	36.4	16.7	31.9
8		20	125.7	45	0.1346	3.33	13.8	1.84	4.80
9		40	125.7	45	0.1346	7.80	16.4	3.90	5.89
10		55	125.7	45	0.1346	9.40	16.1	4.90	6.58
11		20	125.7	AP	0.5734	6.55	27.9	6.20	24.6
12	11.34	35	86.40	60	0.3975	11.3	21.6	10.8	21.7
13		40.5	90.72	60	0.3975	13.5	24.0	14.0	24.3
14		40.5	90.72	55	0.5080	14.9	26.5	11.1	20.0
15		45	119.6	55	0.2355	15.7	25.4	11.4	19.2
16		45	119.6	55	0.2753	17.3	28.0	12.0	21.2
17		15	141.4	45	0.2753	5.00	28.1	2.10	10.5
18		25	141.4	45	0.2753	11.2	32.1	4.50	12.2
19		45	141.4	45	0.2753	22.0	35.2	8.40	13.6
20		60	141.4	45	0.2753	27.1	36.6	10.3	13.6
21	11.40	35	86.40	60	0.3975	11.9	23.4	12.0	23.0
22		25	141.4	45	0.2753	12.3	34.2	4.64	13.0
23		41	141.4	45	0.2753	21.8	37.1	7.90	14.1

For the probe shapes for which the body sonic point occurs at the aft corner ($\theta_c > 50°$), a single-strip method of integral relations program for arbitrary equilibrium gas mixtures[3] was used. When the sonic point occurs on the spherical section and the cone surface is supersonic, an inverse blunt body solution coupled with the method of characteristics was used.[4] The latter calculation was made for pure CO_2 in equilibrium. All the other calculations correspond to the Venus model atmosphere presented in Ref. 5 for which the chemical composition is 97% CO_2 and 3% N_2 by volume.

With the inviscid conditions defined, a boundary-layer solution was performed including the important effect of entropy layer swallowing.[6] The radiative heat flux to the wall from an isothermal slab was calculated using the method of Nicolet.[7] The temperature and pressure of the slab were taken to be the boundary layer edge values at the body point of interest, including entropy layer swallowing, and its thickness was assumed equal to the adiabatic shock standoff distance from the inviscid analysis. Use of the boundary-layer edge temperature rather than the post shock value makes little difference in radiative heating results in the stagnation region or in the cone region for large angle cones. As the cone angle decreases, however, the temperature difference across the shock layer becomes increasingly large in contrast to the pressure difference. As a result, use of the boundary-layer edge temperature in the isothermal slab analysis leads to a somewhat conservative predicted radiative flux, while use of the post shock temperature significantly underpredicts the cone radiative heating for small cone angles. The radiative flux computed by the isothermal slab model was modified by the cooling factor shown in Fig. 1 to

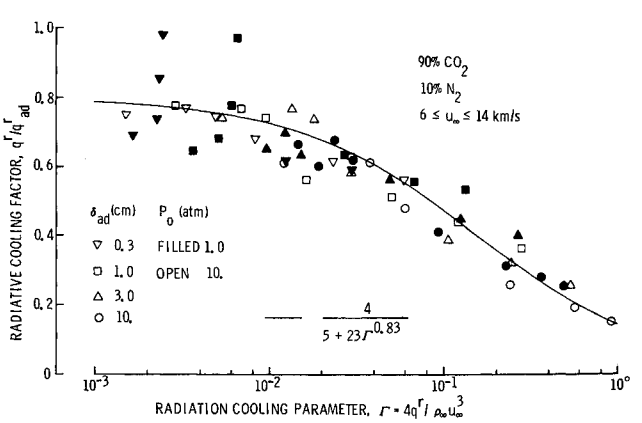

Fig. 1 Radiative cooling factor for Venus entry.